NEUROSCIENCE

Dissociable components of attention exhibit distinct neuronal signatures in primate visual cortex

Adithya Narayan Chandrasekaran[1]†‡, Ayesha Vermani[1]†§, Priyanka Gupta[1], Nicholas Steinmetz[2]‖, Tirin Moore[2,3], Devarajan Sridharan[1,4]*

Attention can be deployed in multiple forms and facilitates behavior by influencing perceptual sensitivity and choice bias. Attention is also associated with a myriad of changes in sensory neural activity. Yet, the relationship between the behavioral components of attention and the accompanying changes in neural activity remains largely unresolved. We examined this relationship by quantifying sensitivity and bias in monkeys performing a task that dissociated eye movement responses from the focus of covert attention. Unexpectedly, bias, not sensitivity, increased at the focus of covert attention, whereas sensitivity increased at the location of planned eye movements. Furthermore, neuronal activity within visual area V4 varied robustly with bias, but not sensitivity, at the focus of covert attention. In contrast, correlated variability between neuronal pairs was lowest at the location of planned eye movements, and varied with sensitivity, but not bias. Thus, dissociable behavioral components of attention exhibit distinct neuronal signatures within the visual cortex.

INTRODUCTION

Attention is a fundamental cognitive function but is not a unitary phenomenon (*1*–*4*). Selective attention facilitates behavior through at least one of two distinct behavioral mechanisms: enhancing perceptual sensitivity, i.e., improving sensory processing of task-relevant information, and enhancing choice bias, i.e., providing an advantage to task-relevant information during behavioral decisions (*5*–*9*). Attentional effects on sensitivity and bias are quantified using the framework of signal detection theory (SDT) with d' and β parameters, respectively (*8*, *10*). Although the neural correlates of attention have been thoroughly investigated, the specific neural mechanisms mediating sensitivity and bias remain controversial (*6*, *11*–*13*).

Attention is associated with diverse effects on neural activity, and these effects have been widely studied in the primate visual system. Two well-documented effects of attention include the enhancement of neuronal firing rates (FRs), often manifesting as a "multiplicative gain" on visual responses (*14*–*16*), and a decrease in "noise" correlations among unit pairs (*17*–*20*). To date, it remains unclear whether these distinct neural signatures reflect the control of common, overlapping, or distinct brain mechanisms. It also remains unknown whether these neural signatures reflect distinct behavioral components. One tantalizing possibility is that the distinct neural signatures of attention map on to distinct components of attention, namely, perceptual sensitivity and choice bias. Whereas the enhancement of neural responses may provide a preferential bias for selected neural representations to drive downstream decision-making (*5*), reductions in noise correlations may improve the quality of sensory representations and may, therefore, improve perceptual sensitivity (*21*). Evidence from one previous study suggests that neuronal modulations in visual cortex during covert spatial attention reflect changes in behavioral sensitivity alone (*13*).

In addition to its distinct behavioral components and apparent diverse neural correlates, it is well known that attention can be deployed in a myriad of ways (*22*, *23*). Spatial attention, for example, can be deployed covertly, in the absence of orienting movements, or it can be deployed overtly, for example, with eye movements (saccades) that target attended objects. To date, a wealth of psychophysical and neurophysiological evidence indicates a strong interdependence between the perceptual effects of covert attention and the neural circuits controlling gaze (*24*–*29*). Yet, recent evidence suggests that these two forms of attention may produce distinct perceptual effects (*30*), when they are experimentally dissociated. When covert attention and saccade planning are dissociated, neurons within the visual cortex (area V4) exhibit FR modulations for both types (*31*). Moreover, there is some evidence that different subpopulations of neurons in the parietal cortex contribute to each type of attention distinctly (*32*, *33*). Yet, given that the vast majority of previous studies of neural signatures of attention did not control for eye movement planning (*12*, *13*, *15*, *17*, *19*, *34*–*38*), it is likely that the correlates described thus far reflect a combination of mechanisms involved in covert attention and gaze control.

In this study, we investigated neural signatures underlying distinct behavioral components of attention—sensitivity and bias—and two forms of attention—covert and gaze related. We used a spatially cued attention task (Fig. 1A) (*15*, *17*, *39*) and analyzed behavior using a recently developed multidimensional SDT model [the multialternative detection/change-detection (m-ADC) model; Fig. 1B] (*6*, *10*), which was designed specifically for quantifying sensitivity and bias in standard attention tasks (*2*). Moreover, in contrast to most previous studies (*12*, *13*, *19*, *34*, *40*), our task dissociated the focus of covert attention from the focus of planned eye movements (Fig. 1A). Our results reveal that distinct forms of attention (covert and gaze related) modulate distinct behavioral

[1]Centre for Neuroscience, Indian Institute of Science, Bangalore, KA, India. [2]Department of Neurobiology, Stanford University School of Medicine, Stanford, CA, USA. [3]Howard Hughes Medical Institute, Stanford University, Stanford, CA, USA. [4]Computer Science and Automation, Indian Institute of Science, Bangalore, KA, India.
*Corresponding author. Email: sridhar@iisc.ac.in
†These authors contributed equally to this work.
‡Present address: Department of Neuroscience and Center for the Neural Basis of Cognition, University of Pittsburgh, Pittsburgh, PA, USA.
§Present address: Champalimaud Centre for the Unknown, Champalimaud Foundation, Lisbon, Portugal.
‖Present address: Department of Biological Structure, University of Washington, Seattle, WA, USA.

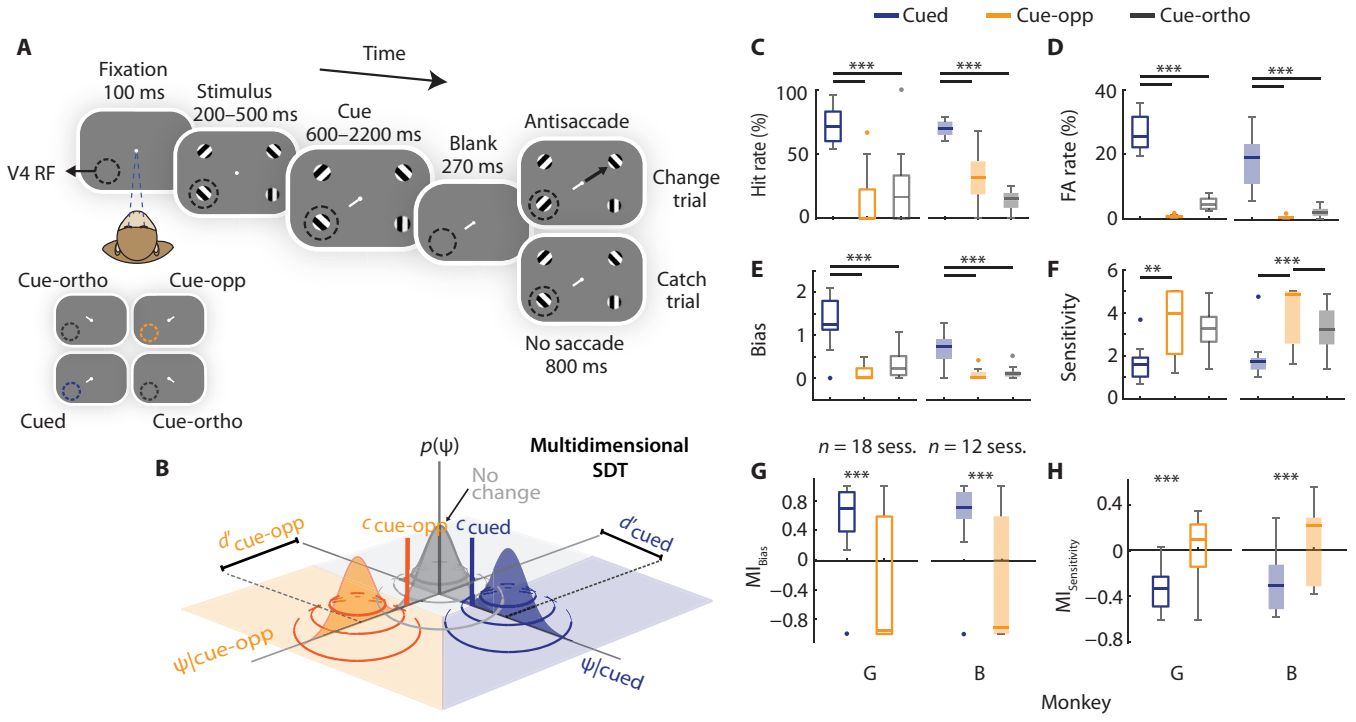

Fig. 1. Spatial cueing and saccade planning produce dissociable effects on choice bias and sensitivity. (**A**) Multialternative change detection task (see the main text for details). Dashed circle: V4 RF. Color and naming conventions: Blue: cued location. Orange: diagonally opposite to cued location (cue-opposite). Gray: contralateral or ipsilateral to cued location (cue-orthogonal). (**B**) m-ADC model for quantifying sensitivity and bias at each location (see the main text for details). Decision variables, denoted by ψ, quantifying evidence for change at the cued location (blue) and an uncued location (orange) are represented along orthogonal (*x* and *y*) axes; the vertical (*z*) axis represents the probability density of the decision variable [$p(\psi)$]. Thick gray lines: decision boundaries that delineate the space into distinct decision zones, corresponding to change at cued location (blue shading), uncued location (orange shading), or no change (gray shading). Blue and orange vertical lines correspond to criteria at the cued and cue-opposite locations, respectively. (**C**) Hit rates at the cued, cue-opposite, and cue-orthogonal locations for monkey G (open boxplots, $n = 18$ sessions) and monkey B (filled boxplots, $n = 12$ sessions). (**D**) Same as in (C) but showing false-alarm rates. Other conventions are as in (C). (**E**) Same as in (C) but showing choice bias. (**F**) Same as in (E) but showing sensitivity. Other conventions are as in (E). (**G**) Modulation index of choice bias (MI_{Bias}) at the cued and cue-opposite locations. (**H**) Same as in (G) but showing MI of sensitivity ($MI_{Sensitivity}$). All panels. Asterisks: significance levels (*$P < 0.05$, **$P < 0.01$, and ***$P < 0.001$). Significance levels for (C) and (D) are based on Wilcoxon signed rank test. Significance levels for (E) to (H) are based on permutation tests.

components (bias and sensitivity, respectively) and are associated with distinct neuronal signatures (FR and noise correlations, respectively) within the visual cortex (area V4).

RESULTS

Spatially dissociating behavioral components of attention

Monkeys performed a cued attention task (*2*, *17*, *39*) in which they detected changes in visual stimuli and responded to those changes with an antisaccadic response (Fig. 1A; Materials and Methods) (*31*). Briefly, each trial began with the monkey fixating a central white dot for 100 ms. This was followed by the appearance of four oriented gratings, one in each visual quadrant. After a variable delay, a spatial cue—a white line segment (<0.5° in length and <0.1° in width) pointed toward one of the four locations—was presented centrally. The cue remained on the screen for a variable interval (600 to 2200 ms, "cue epoch") after which the stimuli disappeared briefly (typically, 270 ms). Upon reappearance, either one of the gratings had changed in orientation ("change trials") or none of the gratings had changed in orientation ("no-change or catch trials"). On change trials, monkeys were rewarded for making a saccadic eye movement to the stimulus diametrically opposite ("antisaccade") to the location of changed stimulus within 800 ms. On catch trials, animals were rewarded for maintaining fixation throughout the response period.

We refer to the location indicated by the cue as the "cued" location, the location opposite the cued location as the "cue-opposite" location, and the two other, uncued locations as "cue-orthogonal" locations (Fig. 1A). Because cue validity was high (90 to 93% on change trials), changes occurred mainly at the cued location on change trials, and saccades occurred primarily toward the cue-opposite location. In other words, the cue-opposite location was the most likely location of saccades, and the cued location was the most likely location of a change. The cue-orthogonal locations served as control conditions for calculating changes in neural activity and psychophysical parameters induced by cueing and saccade planning.

When analyzing neural activity, we refer to trials in which the cued location overlapped with the receptive fields (RFs) of the recorded neurons as the "cued condition." In this condition, we expect that neural activity was influenced by spatial cueing of attention but not by saccade preparation. Similarly, we refer trials in which the cue-opposite location overlapped with the recorded neurons' RFs as the "cue-opposite condition." In this condition, we expect that

neural activity was influenced by saccade preparation but not by spatial cueing. Trials in which the neural RFs overlapped with the cue-orthogonal location served as a control condition ("cue-orthogonal condition") for calculating changes in neural activity and psychophysical parameters induced by cueing and saccade planning.

Each monkey's behavioral responses in the task were organized into a 5 × 5 stimulus-response contingency table (fig. S1A). Psychophysical parameters—sensitivity (d') and criterion (c) at each of the four locations—were estimated by fitting behavioral responses with a multidimensional signal detection model, the m-ADC model, designed specifically for the analysis of such multialternative attention tasks with probabilistic cueing (Fig. 1B) (*6*, *10*). Choice bias was quantified with the likelihood ratio measure (β) (*41*). We extended the m-ADC model to incorporate a response bias component, which accounted for the animals' oculomotor biases when performing the antisaccade task (figs. S1B and S2, A and B) (see the "m-ADC model fitting" section). Goodness-of-fit tests confirmed successful model fits to both monkeys' behavioral responses in this multialternative attention task (fig. S2C). The antisaccade task design permitted distinguishing choice bias for reporting changes at a location from an oculomotor response bias for saccades toward that location.

Monkeys exhibited the highest proportion of "hits" and "false alarms" at the cued location, compared to the other locations (Fig. 1, C and D) [monkey G: $P < 0.001$ and monkey B: $P < 0.001$, for both cued versus cue-opposite and cued versus cue-orthogonal locations; analysis of variance (ANOVA), followed by Tukey-Cramer test]. As a consequence of higher hit and false-alarm rates, choice bias (β) was also highest at the cued location in both monkeys (Fig. 1E) (monkey G: $P < 0.001$, monkey B: $P < 0.001$; permutation test; Materials and Methods). In contrast, sensitivity was higher at the cue-opposite location as compared to the cued location (Fig. 1F) (monkey G: $P = 0.008$, monkey B: $P < 0.001$).

We quantified the effects on d' and β with a "modulation index" (MI), computed as the ratio of the difference of the value of each parameter between the cued (or cue-opposite) and cue-orthogonal locations to its sum [e.g., $(\beta_{cued} - \beta_{ortho})/(\beta_{cued} + \beta_{ortho})$]. We observed significantly higher bias modulation (MI-β) at the cued compared to the cue-opposite location in both monkeys (Fig. 1G) (monkey G: $P < 0.001$, monkey B: $P < 0.001$) but significantly higher sensitivity modulation (MI-d') at the cue-opposite, compared to the cued, location (Fig. 1H) (monkey G: $P < 0.001$, monkey B: $P < 0.001$). We repeated these analyses with a similarity choice model (*42*) and observed nearly identical sensitivity and bias effects at all locations (fig. S3, A and B). These behavioral results indicate that spatial probabilistic cueing of attention did not produce an increase in sensitivity (d') at the cued location when that location was dissociated from the location of planned eye movements, in our task. Choice bias, but not sensitivity, was highest at the cued location, despite this location being cued for attention, whereas sensitivity was highest at the cue-opposite location, toward which saccades were most likely. This latter result provides evidence in monkeys of a classic result previously shown in human subjects, namely, of the obligatory coupling of sensitivity to the location of planned eye movements (*24*, *25*).

Last, we also quantified the oculomotor (saccadic) response bias or motor bias (Materials and Methods), which reflects the animals' bias to make saccades toward a location. As expected, motor bias was highest toward the cue-opposite location, the most likely location for saccades (fig. S1C) (monkey G: $P < 0.001$, monkey B: $P < 0.001$, for both cue-opposite versus cued and cue-opposite versus cue-orthogonal locations). Nevertheless, microsaccades—small fixational eye movements <1° in amplitude (*43*, *44*)—were systematically biased toward the cued location. To quantify directional biases in microsaccades, we computed the summed magnitude of the projection of microsaccade vectors toward each location, across trials: A higher value of this metric at any location indicates a larger magnitude and/or a higher frequency of microsaccades, reflecting a greater propensity for microsaccades toward that location (see the "Microsaccade detection algorithm" section). The microsaccade MI (MI-μs, defined, as before, relative to the orthogonal locations as baseline), computed in a window from 250 to 750 ms after cue onset, was significantly higher toward the cued location as compared to the cue-opposite location (monkey G, $P = 0.005$ and monkey B, $P = 0.001$).

At first glance, it is unusual that choice bias, but not sensitivity, was highest, at the cued location. However, this result can be explained by a behavioral strategy specific to probabilistically cued attention tasks (*2*). Model simulations of such a task revealed that decreasing the criterion (increasing choice bias) at the cued location relative to the uncued location, without altering sensitivities, was sufficient to produce robust, overall increases in percent correct (fig. S4, A to C) (see the "Effect of criterion changes on overall accuracy in multialternative detection tasks" section). Next, we explored the neural correlates of these behavioral effects on bias and sensitivity induced, respectively, by spatial cueing and saccade planning. Specifically, we analyzed two well-documented neural signatures of attention: the modulation of V4 neuronal FRs (*14*) and pairwise noise correlations (*18*).

FRs vary with bias, not sensitivity, during covert attention

First, we analyzed the effect of spatial cueing and saccade planning on V4 neuronal FRs. For this, we computed the FRs for each V4 unit ($n = 464$ units, 297 in monkey G and 167 in monkey B) in 500-ms moving windows and calculated an MI (MI_{FR}; Materials and Methods) that quantified the change in FRs during trials when the RF was at the spatially cued location, referred to as the cued condition, or at the cue-opposite (saccade target) location, referred to as the cue-opposite condition, relative to the cue-orthogonal (control) conditions [e.g., $MI_{FR\text{-}cued} = (FR_{cued} - FR_{ortho})/(FR_{cued} + FR_{ortho})$]. V4 FRs increased significantly for both the cued and the cue-opposite conditions, as previously described (*31*). The MI_{FR} was positive during the cue epoch (500 ms after cue onset until blank onset; Fig. 2A), and median MI_{FR} was significantly greater than zero for both the cued and cue-opposite conditions (MI_{FR}: cued $= 0.82 \pm 0.45 \times 10^{-2}$, $P = 0.001$, Wilcoxon signed rank test, Bayes factor = 1.90; cue opposite: $2.29 \pm 0.49 \times 10^{-2}$; $P < 0.001$, Bayes factor = 243.11) (Fig. 2B). Despite heterogeneity in this pattern of responses among individual units, a substantial proportion of units showed a positive MI_{FR} for both conditions (~44%), and the vast majority (~75%), for at least one of the two conditions (fig. S5B). MI_{FR} exhibited different dynamics between the cued and cue-opposite conditions. For the cued condition, MI_{FR} increased robustly and plateaued following cue onset, whereas MI_{FR} for the cue-opposite condition ramped up continuously throughout in the cue epoch (Fig. 2A); this trend was consistent across both monkeys (fig. S5A). In other words, V4 FRs were enhanced both when the RF was at the location of highest bias (covert attention) and when the RF was at the location of highest

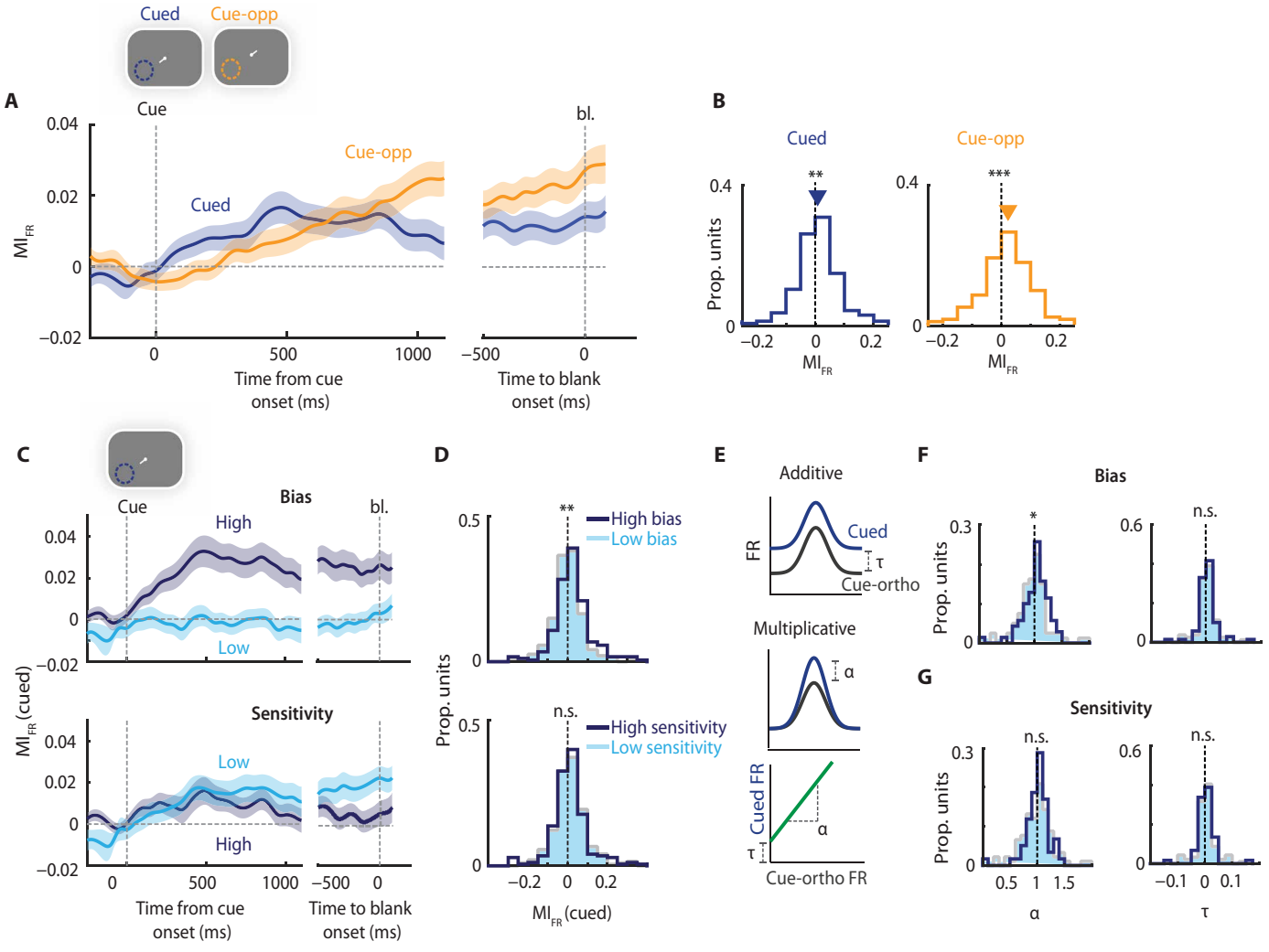

Fig. 2. Firing rates vary selectively with bias at the covertly attended location. (**A**) Left: Time evolution of FR MI of V4 units (mean V4 MI_{FR}) locked to cue-onset (cue, dashed vertical line), for the cued (blue) and cue-opposite (orange) conditions. Dashed horizontal line: $MI_{FR} = 0$. Shaded region: SEM ($n = 464$ units). MI_{FR} was calculated in 500-ms moving windows (50-ms shift; interpolated with 5-ms resolution). Right: Same as in the left panel but locked to blank onset (bl., dashed vertical line). (**B**) Distribution of V4 MI_{FR} values for the cued (left) and cue-opposite (right) conditions, computed in a window from 500 ms after cue onset until the end of cue epoch. n.s., not significant. (**C**) Time evolution of V4 MI_{FR} for the cued condition, for high-bias (dark blue; $n = 221$ units) and low-bias (light blue; $n = 243$ units) sessions (top) and for high d' ($n = 219$ units) and low d' ($n = 245$ units) sessions (bottom). (**D**) Distribution of V4 MI_{FR} values for the cued condition for high-bias and low-bias sessions (top) and for high d' and low d' sessions (bottom). (**E**) Schematic showing additive shift (top, denoted by τ) and multiplicative gain (middle, denoted by α) modulation of tuning curves. Bottom: Linear model for calculating intercept (τ/additive) and slope (α/multiplicative) parameters (see the main text for details). (**F**) Distribution of α for the high-bias ($n = 70$ units) and low-bias ($n = 80$ units) sessions (left) and distribution of τ for high-bias and low-bias sessions (right). (**G**) Distribution of α, separately for the high d' ($n = 59$ units) and low d' ($n = 91$ units) sessions (left) and distribution of τ for high d' and low d' sessions (right).

sensitivity (saccade target), but they exhibited qualitatively different temporal dynamics.

Next, we tested whether V4 neuronal activity varied with either sensitivity or bias changes. Because signal detection model parameters d' and β cannot be estimated with single trial responses, we labeled entire sessions as "high" or "low," based on a median split of either bias (β-split) or sensitivity (d'-split) for the cued condition (Materials and Methods) (fig. S2, D and E). We then compared the modulation of V4 FRs across sessions with high or low values of the respective psychophysical parameter. Figure 2C shows the time-resolved FR modulation (MI_{FR}) during the cue epoch for each group of sessions. V4 activity modulated systematically with bias. The modulation was significantly higher during sessions with high bias than those with low bias during the cued condition (Fig. 2C, top, and Fig. 2D, top) (β-split: median $\Delta MI_{FR} = 1.36 \times 10^{-2}$, Cohen's $d = 0.253$, $P = 0.002$, Mann-Whitney U test, Bayes factor = 3.84). This effect was also consistent in a window-computed 400 ms before the blank onset (Cohen's $d = 0.312$, $P < 0.001$, Bayes factor = 25.05). Moreover, the pattern of FR modulations was similar in each monkey (fig. S6, A and B).

In addition, we tested whether the FR modulation reflected shifts in tuning curve baseline (additive modulation), scaling of amplitude (multiplicative modulation), or a combination of both (*45*), by fitting a linear model for the FR responses at the cued versus

cue-orthogonal locations across different stimulus orientations (see the "Tuning curve analysis" section) (Fig. 2E). We found a significantly higher slope (α) for the high-bias, as compared to low-bias sessions (β-split: median $\Delta MI\alpha = 7.43 \times 10^{-2}$, $P = 0.027$) (Fig. 2F, left), indicative of a multiplicative modulation. On the other hand, the intercept (τ), which quantifies the degree of additive (baseline) shift, was not significantly different across the two session types (median $\Delta MI\tau = -0.10 \times 10^{-2}$, $P = 0.935$) (Fig. 2F, right). We confirmed these results also by fitting a Gaussian model with amplitude (A), mean (μ), width (σ), and baseline (b) parameters (fig. S6, C to F). Thus, FR modulations with bias were best explained by a multiplicative gain modulation.

In contrast to clear effects of bias, V4 FR exhibited no clear modulation with sensitivity for the cued condition (d'-split: median $\Delta MI_{FR} = -0.22 \times 10^{-2}$, Cohen's $d = -0.057$, $P = 0.614$, Bayes factor = 0.12) (Fig. 2C, bottom, and Fig. 2D, bottom). We observed similar effects in a window 400 ms before the blank onset (Cohen's $d = -0.176$, $P = 0.047$, Bayes factor = 0.57). In addition, neither tuning curve parameter (slope and intercept) modulated significantly with d' (d'-split: median $\Delta MI\alpha = -2.20 \times 10^{-2}$, $P = 0.474$, $\Delta MI\tau = -3.4 \times 10^{-4}$, $P = 0.559$) (Fig. 2G). Thus, neuronal orientation tuning functions exhibited systematic multiplicative gain modulation with bias but not with sensitivity. We also tested for the variation of the Fano factor with sensitivity and bias. This analysis revealed no clear modulation with sensitivity ($P = 0.634$, Bayes factor = 0.13), but a significant modulation with bias such that Fano factor was marginally higher for the high-bias, compared to the low-bias sessions (β-split: median $\Delta MI_{FF} = 1.5 \times 10^{-2}$, $P = 0.009$, Bayes factor = 2.09) (fig. S6G). These results indicate that while mean FRs increased with bias, the variance of FRs (noise) also increased, albeit marginally.

Because of the high cue validity (>90%), orientation changes occurred rarely during the cue-opposite condition when the RF was the saccade target location. Thus, there were not sufficient trials to examine whether neuronal activity varied with sensitivity and bias for the (invalid) cue-opposite condition. However, we could nonetheless examine whether activity during the cue-opposite condition covaried with sensitivity and bias during the (validly) cued condition. We found that V4 activity during the cue-opposite condition modulated with sensitivity during the cued condition (Fig. 3A, top, and Fig. 3B, top). V4 activity for the cue-opposite condition was significantly higher, and increased over time, during sessions with low sensitivity at the covertly attended (cued) location, compared to sessions with high sensitivity at the covertly attended location (d'-split/cued: median ΔMI_{FR}/cue-opp $= -2.32 \times 10^{-2}$, Cohen's $d = -0.2927$, $P < 0.001$). In contrast, no such systematic differences were apparent in the data split by bias for the cued condition (Fig. 3A, bottom, and Fig. 3B, bottom; $P = 0.153$). Thus, greater activity at the location of planned saccades was negatively correlated with sensitivity at the diametrically opposite location of covert spatial attention.

Last, we analyzed laminar differences in FRs across superficial and deep V4 layers, demarcated based on the current source density (CSD); in these analyses, the superficial compartment included what was likely input layer IV (Materials and Methods; fig. S7A) (*19*, *46*). Superficial ($n = 169$) and deep ($n = 295$) layer activity was robustly modulated by saccade planning during the cue-opposite condition (superficial $MI_{FR} = 2.75 \pm 0.59 \times 10^{-2}$; $P < 0.001$; deep $MI_{FR} = 2.07 \pm 0.69 \times 10^{-2}$, $P = 0.001$) (Fig. 4A, right, and Fig. 4B, right). However, only the superficial-layer activity was modulated by covert attention (superficial $MI_{FR} = 1.69 \pm 0.59 \times 10^{-2}$; $P < 0.001$; deep $MI_{FR} = 0.42 \pm 0.63 \times 10^{-2}$, $P = 0.134$) (Fig. 4A, left, and Fig. 4B, left). Laminar analysis revealed an additional, interesting dichotomy between superficial- and deep-layer neurons: FRs of superficial-layer neurons, but not deep-layer neurons, varied significantly with bias (superficial: $P = 0.002$, Bayes factor = 32.18; deep: $P = 0.192$, Bayes factor = 0.28) (Fig. 4, C and D). We repeated these analyses for a subset of sessions in which the input layer IV could be clearly demarcated on the basis of CSD markers reported in literature (*19*) (Materials and Methods). FRs of putative layer IV units varied only weakly with bias ($P = 0.11$, Bayes factor = 0.67, $n = 102$) (fig. S7B, top); by contrast, FRs of the remaining units in layers II to IV varied strongly and significantly with bias ($P = 0.003$, Bayes factor = 15.91, $n = 67$) (fig. S7B, bottom).

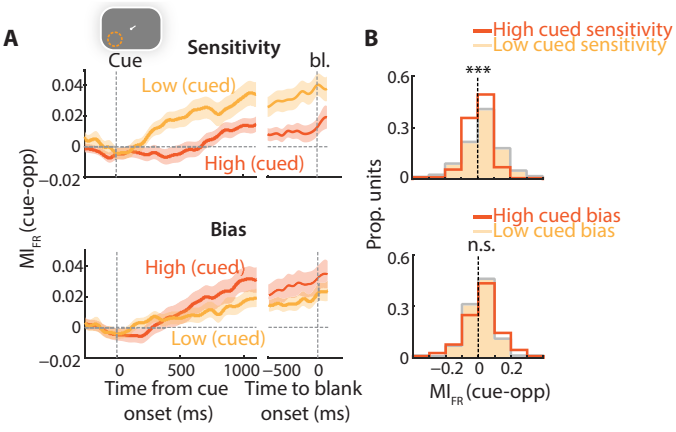

Fig. 3. Firing rates at the saccade target location predict sensitivity at the covertly attended location. (**A**) Top: Same as in Fig. 2C (bottom) but showing V4 MI_{FR} traces for the cue-opposite condition for high d' (dark orange) and low d' (light orange) sessions, split based on the cued condition. Bottom: Same as in the top panel but showing V4 MI_{FR} traces for the cue-opposite condition for high-bias and low-bias sessions, split based on the cued condition. Other conventions are the same as in Fig. 2C. (**B**) Top: Same as in Fig. 2D (bottom) but showing the distribution of V4 MI_{FR} values for the cue-opposite condition for high d' and low d' sessions, split based on the cued condition. Bottom: Same as in the top panel but showing the distribution of V4 MI_{FR} values at the cue-opposite condition for high-bias and low-bias sessions, split based on the cued condition.

Together, these results show that when the focus of covert attention was decoupled from saccade planning, V4 neuronal activity modulated selectively with bias, but not sensitivity, for the covertly attended (cued) condition. The FR changes were best described by a multiplicative gain modulation of orientation tuning. FR modulation at the saccade target location was predictive of sensitivity during the cued condition when the RF was at the covertly attended location. In addition, only superficial-layer unit activity was significantly modulated by both covert attention and bias, indicating that neural mechanisms mediating bias changes during covert spatial attention are distinct from those underlying saccade planning.

Noise correlations vary with sensitivity but not bias

Next, we measured spike-count ("noise") correlations between pairs of V4 units during the cue epoch and examined how these modulated with covert attention and saccade planning. Previous studies reported a reduction in noise correlations at the attended location (*17*, *18*) in a manner that appears to facilitate sensory decoding of

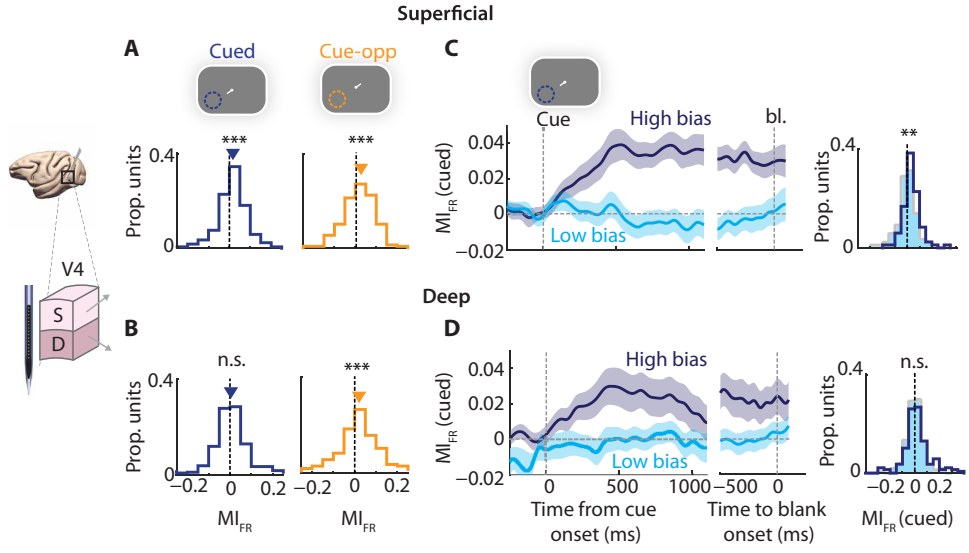

Fig. 4. Firing rates of only superficial layers vary with bias at the covertly attended location. (**A**) Same as in Fig. 2B but showing MI_{FR} of V4-superficial layer units ($n = 169$ units) for cued (left) and cue-opposite (right) conditions. Other conventions are the same as in Fig. 2B. (**B**) Same as in (A) but showing MI_{FR} of V4 deep-layer units ($n = 295$ units). (**C**) Left: Same as in Fig. 2C (top) but showing MI_{FR} for V4 superficial layer units for high-bias ($n = 83$ units) and low-bias ($n = 86$ units) sessions. Right: Same as in Fig. 2D (top) but showing distribution of MI_{FR} values for V4 superficial layer units. (**D**) Left: Same as in [(C), left] but showing MI_{FR} for V4 deep-layer units for high-bias ($n = 138$ units) and low-bias ($n = 157$ units) sessions. Right: Same as in [(C), right] but showing distribution of MI_{FR} values for V4 deep-layer units. [(A) to (D)] Color conventions are the same as in Fig. 2.

the attended stimulus (*47*); this effect appears to be strongest within the more superficial layers (*19*). Although these results suggest that covert attention reduces correlated variability, none of the previous studies dissociated covert attention from oculomotor planning. Previous studies have not directly linked the modulation of noise correlations with psychophysical metrics of d' and bias. Thus, we examined noise correlations for the two dissociated conditions, separately.

Noise correlations increased monotonically with the mean evoked response, for both the cued and cue-opposite conditions (Fig. 5A), consistent with previous studies (*18*). The MI of the noise correlation ($MI_{r\text{-}sc}$) for the cue-opposite condition was significantly lower than for the cued condition ($\Delta MI_{r\text{-}sc} = 8.56 \pm 2.0 \times 10^{-2}$, $P < 0.001$, permutation test; Bayes factor = 214.59) (Fig. 5B). Moreover, in comparison to the control (orthogonal) conditions, noise correlations were significantly higher for the cued condition (Fig. 5B) ($MI_{r\text{-}sc}$: cued $= 4.25 \pm 1.73 \times 10^{-2}$, $P = 0.006$, sign-rank test). In addition, the patterns of noise correlation effects reflected specific behavioral d' trends in each of the two monkeys (fig. S8, A and B), suggesting a correspondence between perceptual sensitivity modulation and reduced noise correlations in V4 activity.

In addition, noise correlations covaried with perceptual sensitivity variations. As in the FR analysis, we divided sessions based on a median split of the respective psychophysical parameter (d' and β) value during the cued condition and tested whether noise correlations were significantly different across the two session groups. In contrast to the trend observed with FRs, noise correlations varied systematically with sensitivity: $MI_{r\text{-}sc}$ computed in a 400-ms window preceding blank onset (Materials and Methods) was significantly lower for the high d' sessions, as compared to the low d' sessions (d' split: Cohen's $d = -0.179$, $P < 0.001$, Bayes factor = 5.47) (Fig. 5C). On the other hand, noise correlations computed during the same window did not vary significantly across high-bias and low-bias sessions (β-split: median Cohen's $d = -0.064$, $P = 0.11$, Bayes factor = 0.11) (Fig. 5D). In other words, at the location of covert attention, noise correlations in V4 were predictive of sensitivity but not bias.

Last, laminar analysis revealed a specific dichotomy between superficial- and deep-layer neurons. In the superficial layers, noise correlations did not differ between the cued and the cue-opposite conditions ($\Delta MI_{r\text{-}sc} = 3.4 \pm 4.01 \times 10^{-2}$, $P = 0.263$, Bayes factor = 0.10) (Fig. 5E); these results were unchanged when putative layer IV units were analyzed separately (putative layer IV: $\Delta MI_{r\text{-}sc} = 5.42 \pm 4.76 \times 10^{-2}$, $P = 0.786$, Bayes factor = 0.17). However, within the deeper layers, the contrasting noise correlation effects were more prominent, and differed significantly ($\Delta MI_{r\text{-}sc} = 14.43 \pm 3.58 \times 10^{-2}$, $P < 0.001$, Bayes factor = 135.42) (Fig. 5F). In addition, the suppression of noise correlations at the cue-opposite condition relative to baseline (cue-orthogonal conditions) was statistically significant for the deep-layer units (Fig. 5F, orange bar, $P = 0.002$, Wilcoxon signed-rank test, Bayes factor = 11.08). The above results show that when the target of the eye movement response is spatially dissociated from the focus of covert attention, the expected decreases in noise correlations during covert attention disappear. Instead, reductions in noise correlation were associated with the planning of saccadic eye movements, specifically in the deep layers. Furthermore, noise correlations modulated robustly with sensitivity, but not bias, indicating that saccade planning may engage this specific neural mechanism for controlling perceptual sensitivity.

In summary, dissociating covert attention from saccade planning enabled dissociating distinct components of attention—bias and sensitivity—across spatial locations. Whereas bias was highest when the RF was at the focus of covert attention, sensitivity was highest when the RF was at the location of planned eye movements. V4 FR modulations at the covertly attended location emerged as a specific signature of bias, but not sensitivity, and were most prominent in

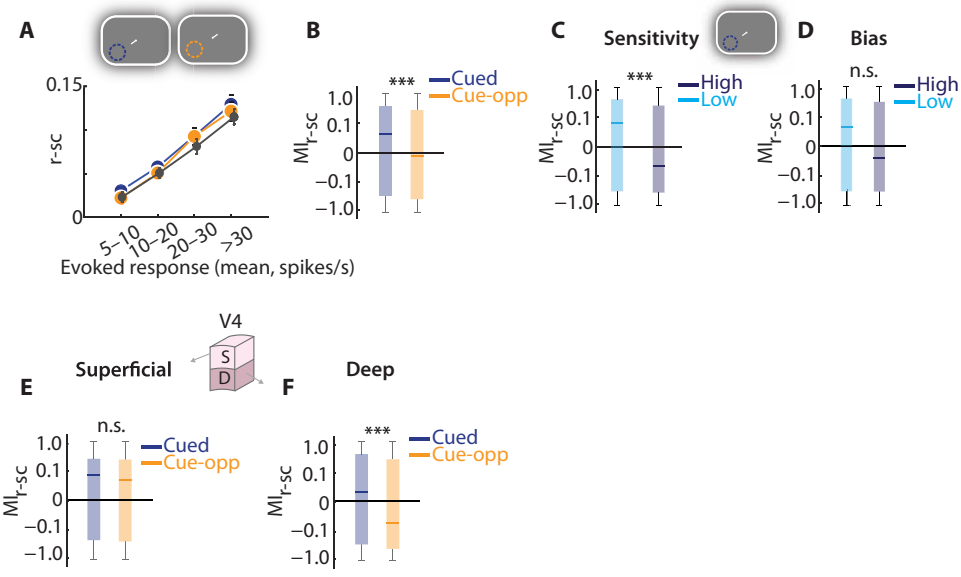

Fig. 5. Noise correlation changes in the deep layers specifically reflect sensitivity changes. (**A**) Noise correlation (r-sc) between pairs of V4 units for the cued (blue), cue-opposite (orange), and cue-orthogonal (gray) conditions as a function of the pairwise geometric mean of evoked responses. Error bars: SEM ($n = 1559$ unit pairs). (**B**) Modulation index of noise correlation ($MI_{r\text{-}sc}$) for the cued and cue-opposite conditions across all unit pairs shown in (A). The *y* axis is in symmetric logarithm scale. Other conventions are as in (A). (**C**) $MI_{r\text{-}sc}$ for high *d′* (dark blue; $n = 639$ pairs) and low *d′* (light blue; $n = 920$ pairs) sessions, based on the cued condition. Other conventions are as in (B). (**D**) Same as in (C) but showing $MI_{r\text{-}sc}$ for high-bias ($n = 806$ pairs) and low-bias ($n = 753$ pairs) sessions, based on the cued condition. (**E**) Same as in (B) but showing $MI_{r\text{-}sc}$ for V4 superficial layer unit pairs ($n = 251$ unit pairs). (**F**) Same as in (D) but showing $MI_{r\text{-}sc}$ for V4 deep-layer unit pairs ($n = 561$ unit pairs). [(A) to (F)] Color conventions are the same as in Fig. 2.

superficial layers. The FR modulations could be best accounted for by a multiplicative gain of V4 tuning curves. In contrast, the reduction in noise correlations in V4 occurred only when the RF was at the saccade target location and was significant only in deep layers. Moreover, noise correlations varied systematically with sensitivity but not bias. Our results show that distinct forms of attention, covert and gaze related, modulate distinct behavioral components (bias and sensitivity, respectively), which map on to distinct neuronal signatures within the visual cortex.

DISCUSSION

We used a standard, multialternative, endogenous attention task with spatial probabilistic cueing and quantified sensitivity and bias at different spatial locations with a recent multidimensional SDT model, specifically designed for the analysis of such tasks (*6*, *10*). Unlike previous tasks that coupled the location of attention with the location of planned eye movements, in our task, the location of the cue was dissociated from (but not independent of) the location of the saccade. Even tasks that incorporate a non-oculomotor response [e.g., lever release (*40*)] are not immune to this pitfall. For example, it is likely that saccade planning occurs naturally toward the cued location even in such tasks (*24*, *48*). Without directly measuring eye movement plans, it is not possible to ensure that the locus of cued attention and saccade planning are indeed dissociated.

By contrast, the antisaccade paradigm in our task strongly encouraged saccade planning away from the cued location, as evidenced by a substantial proportion of early saccades toward the cue-opposite location. This enabled us to dissociate and directly compare the distinct effects of spatial cueing and saccade preparation on perceptual sensitivity and choice bias (*49*, *50*). We observed that when the focus of covert attention and saccade planning were dissociated, sensitivity and bias were also spatially dissociated. Sensitivity was highest at the cue-opposite location, the most probable location for saccades. These behavioral results are consistent with previous studies in human participants indicating that perceptual sensitivity is largely dependent on saccade planning (*24*, *51*). In contrast, we found that choice bias, but not sensitivity, was highest at the location cued for attention. Interestingly, the pattern of microsaccades during the cue epoch also showed a clear bias toward the cued location (fig. S2F), although the subsequent saccade was typically made to the cue-opposite location. Whereas previous studies have reported a potential link between microsaccades and attention (*44*, *52*), our results suggest that microsaccades may index a particular component of attention (choice bias).

More generally, our results indicate that spatial probabilistic cueing of attention does not produce an increase in sensitivity (*d′*) at the cued location when that location is dissociated from the location of planned eye movements. Instead, cueing can increase choice bias, which is a valid strategy to increase overall performance in probabilistically cued attention tasks (fig. S4). This latter finding is consistent with models in which attention's effects manifest, not in terms of enhanced sensory coding, but in terms of altered decision policies (*53*).

In our study, FRs of area V4 neurons modulated systematically with choice bias but, unexpectedly, not with sensitivity. These results are consistent with previous work by Baruni *et al.* (*54*) who used a spatially biased reward paradigm and found that V4 activity modulations reflected decisional mechanisms (bias changes) rather than signal-to-noise (sensitivity) enhancement mechanisms. Similarly, a

recent study showed that V4 activity robustly encodes choice-related information in perceptual discrimination tasks (*55*).

These observations appear at odds with a recent study by Luo and Maunsell (*13*), which reported that V4 activity modulations during the cue epoch reflect, specifically, sensitivity changes. In this study, the authors dissociated sensitivity from bias with a unique reward manipulation and a change detection (Yes/No) task. Sensitivity and bias were each systematically manipulated across the cued and uncued locations, in distinct sessions, while keeping the other parameter at a fixed value. Sensitivity was manipulated by increasing the magnitude of average reward at one location relative to the other. In contrast, the criterion (bias for detection response) was manipulated by differentially rewarding hits versus correct rejections at each location, while keeping the mean reward the same, across the two locations. Using this reward manipulation, V4 modulation was found to correlate selectively with sensitivity but not with criterion (bias).

A possible explanation for these divergent findings is that criterion changes—induced by differential rewards to different response types—are unrelated to attention [see also Wyart *et al.* (*56*)]. We propose that, in the criterion manipulation sessions, the animal's attention would not have been engaged toward the low criterion location, given that the overall reward was the same across the two locations. Rather, the criterion manipulations induced an expectation of reward, and, therefore, a response bias, for Yes responses at one location (low criterion) and, conversely, a corresponding response bias for No responses at the other location (high criterion). As elegantly demonstrated by a subsequent study (*12*), these response biases could be mediated by prefrontal neurons involved in reward expectation but are unlikely to engage attention at one spatial location selectively.

We also found that when dissociated from saccade preparation, covert attention was not accompanied by reductions in noise correlations in V4 activity. Instead, noise correlations were reduced when saccades were planned to the neuronal RFs. Thus, our results show that distinct forms of attention, covert and gaze-related, are not only associated with distinct behavioral components (bias and sensitivity), but that they map on to distinct neuronal signatures within visual area V4.

Many recent studies have suggested dissociable neural substrates underlying sensitivity and bias. For example, some studies have suggested a specific role for the superior colliculus in modulating bias but not sensitivity (*6*, *11*, *57*, *58*). These results have led to the hypothesis that distinct brain regions, or networks of brain regions, may mediate sensitivity and bias components of attention (*6*, *12*, *59*). Evidence from multiple species indicates that changes in sensory responses and in behavioral performance during spatial attention are driven, at least in part, by gaze control neurons in the prefrontal cortex, specifically the frontal eye field (FEF) (*26*–*29*, *60*). This evidence is consistent with the human psychophysical evidence indicating a strong interdependence of spatial attention and saccade planning (*24*, *25*). Nonetheless, it remains unclear to what extent the behavioral control of attention relies solely on gaze mechanisms. More recent human psychophysical studies indicate that the effects of covert and gaze-related attention on behavior may also be distinct (*30*), thus suggesting that dissociable neural substrates may mediate bias and sensitivity. Our observation that neural correlates of sensitivity and bias are both present within V4, albeit during distinct behavioral states, is consistent with that possibility. It is also possible that distinct subpopulations of neurons within FEF control covert and gaze-related attention. In a standard (prosaccade) attention task, these subpopulations would work in concert producing both bias and sensitivity enhancements at the location cued for attention and eye movements. On the other hand, the antisaccade nature of our task could have induced spatial competition between these subpopulations. Top-down modulations from these FEF subpopulations to distinct covert and gaze-related neural populations in V4 could then mediate the spatially dissociable effects on bias and sensitivity, respectively. In addition, at least some of the effects on FRs and noise correlations occur outside the attentional loci of interest (*61*). In our analyses, we normalized neural activity or behavioral metrics at the two loci of interest (cued and cue-opposite) based on their respective values at the cue-orthogonal locations, along the lines of previous studies (*31*, *62*); the latter locations are neither targets of saccade planning nor spatially cued. A decrease in FRs or an increase in noise correlations at these cue-orthogonal locations could have also contributed to neural modulations reported at the cued and cue-opposite locations. These hypotheses remain to be tested in future studies.

A few previous studies have examined laminar differences in the neural correlates of spatial attention in area V4 (*19*, *46*, *63*). Buffalo *et al.* (*63*) found that covert attention produced comparable effects across layers on FRs and noise correlations; yet, attentional effects on gamma and alpha synchrony were layer specific. In contrast, using higher channel-count electrodes, Nandy *et al.* (*19*), observed a laminar dependence of both FR and noise correlation modulations across layers, with larger effects within the input and superficial layers than in the deep layers. Similarly, Pettine *et al.* (*46*) observed that whereas V4 neurons in superficial layers exhibited greater orientation selectivity, neurons in deep layers conveyed more information about saccade planning. In the present study, reductions in noise correlations were strongest in the deeper layers, particularly at the saccade target location, and covaried with sensitivity changes. Deep-layer neurons project predominantly to lower visual areas including V1 and V2 (*64*–*66*) and the superior colliculus, a key region involved in eye movement control. Recurrent connections between the V4 and these lower visual areas and local processing within them may mediate fine grained feature analysis and, therefore, perceptual sensitivity improvements. By contrast, FR increases by covert attention occurred significantly in the superficial layers. V4 neurons in these layers project to higher visual areas (*65*) and may also preferentially receive top-down input from other cortical areas [e.g., FEF (*67*)]. Top-down inputs to V4 may enable enhancing (biasing) the relevance of visual information at the cued location over other locations.

In summary, these results inspire a mechanistic schema by which distinct neural codes in the visual cortex map on to distinct forms and components of attention. Covert attention induces a multiplicative gain modulation of FRs, especially in the superficial layers; such gain modulation confers a specific advantage for selecting attended stimuli for downstream decision-making (*5*). This neural effect may manifest, behaviorally, as an increase in choice bias (decrease in criterion) at the focus of covert attention (Fig. 6A); this hypothesis is consistent with multiple previous studies that report an increase in neuronal FRs and behavioral bias at the covertly attended location (*6*, *8*, *10*, *31*, *35*, *37*, *58*, *68*–*70*). By contrast, saccade planning yields a reduction in noise correlations, especially in the deep layers; this reduction may improve the quality of sensory representations by

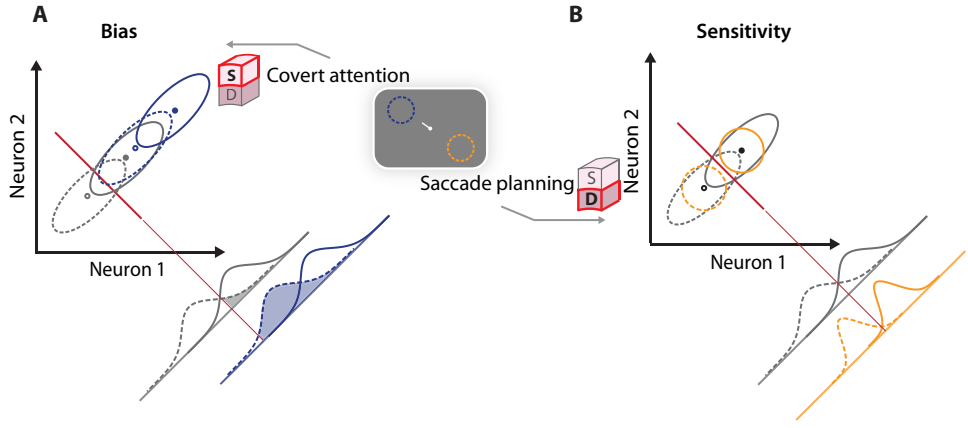

Fig. 6. A schema for sensitivity and bias control by distinct forms of attention. A mechanistic neural schema showing how distinct forms of attention control sensitivity and bias. The *x* and *y* axes represent the neural activity for two hypothetical neurons (1 and 2), respectively. Gray ellipses represent the distribution of neural activity at the unattended (cue-orthogonal) location. Blue and orange ellipses represent the distributions of neural activity at the covertly attended (cued) and the saccade target (cue-opposite) locations. For each location, dotted and solid ellipses represent the responses to the original and changed stimuli, respectively. Thick red lines represent the decision criterion. (**A**) Covert attention induces a multiplicative gain in neuronal FR, primarily in the superficial V4 layers. Such an increase provides an advantage for selected neuronal representations in downstream decision making (increased area of each distribution to the right of the criterion), thereby yielding higher bias for attended information. (**B**) Gaze-related attention (e.g., due to saccade planning) induces a decrease in pairwise noise correlations, prominent in the deeper V4 layers. Such a reduction enables more reliable readout of selected sensory information (lesser overlap between the two distributions along the readout axis), thereby yielding higher sensitivity for distinguishing signal from noise.

reducing the overlap between signal and noise FR distributions along the readout axis. This neural effect translates, behaviorally, into higher perceptual sensitivity (d') (Fig. 6B); this hypothesis is consistent with behavioral reports of increased d' at the location of planned eye movements (*51*, *71*) and also with neural reports of increased orientation discriminability in V4 neurons before saccade onset (*72*). In other words, distinct forms of attention may operate via distinct neural codes to control distinct behavioral components of attention.

MATERIALS AND METHODS

Experimental model and subject details

Data were collected from two male rhesus macaque monkeys (monkey G and monkey B; *Macaca mulatta*, weight: 8 to 12 kg). Experimental procedures were in concordance with the National Institutes of Health *Guide for the Care and Use of Laboratory Animals* and the Society for Neuroscience Guidelines and Policies, and approved by the Stanford University Animal Care and Use Committee. Data analysis protocols were approved by the Institute Human Ethics Committee at the Indian Institute of Science, Bengaluru.

Behavioral and neural data acquisition

Some of the data (behavior and V4 recordings) analyzed for this study were collected as part of a previous study (*31*). This study presents behavioral analyses of these data with signal detection models and the correlation of psychophysical parameters with neural metrics.

Behavioral task and data acquisition

Visual stimuli were displayed on a Samsung 223R3Z monitor at 120 Hz and 1680 × 1050 resolution (17.8 pixels/°). The monitor was positioned at 28.5 cm from the monkey's eyes. Each trial began with the monkey maintaining fixation at a central white dot for 100 ms. This was followed by the appearance of four oriented gratings—full-contrast static Gabor patches, typically, ~4° in diameter and ~1 cycles per degree in spatial frequency—one in each visual quadrant. At each location, the orientation of the gratings was randomly sampled from among 16 evenly spaced values, from 0° to 360° in increments of 22.5°. After a variable delay of 300 to 500 ms, a spatial cue—a white line segment <0.5° in length and <0.1° in width directed toward one of the four locations—was presented centrally. The cue remained on the screen for a variable interval (600 to 2200 ms) following which the stimuli briefly disappeared (270 ms) and reappeared. Upon reappearance, either one of the gratings had changed in orientation (change trials) or none had changed (no-change or catch trials). On change trials, the animals were rewarded for saccading to the stimulus diametrically opposite to the location of change ("antisaccade" response) within a response window of 800 ms. On no-change trials, animals were rewarded for withholding a response and maintaining fixation throughout the response period. We refer to the location opposite the cue as the cue-opposite location and the two other uncued locations as cue-orthogonal locations (Fig. 1A) (*31*). Change and no-change trials occurred in equal proportions (50% each). Cue validity was 90 to 93% on change trials.

For monkey G, data were acquired from 24 behavioral sessions. Of these, three sessions did not contain any invalidly cued trials and were excluded from further analyses. In addition, three sessions were excluded due to partially corrupted eye-tracking data or incomplete V4 recordings. For this study, data were analyzed from the remaining 18 sessions for monkey G. For monkey B, data were acquired from 21 behavioral sessions. Of these, the initial nine behavioral sessions used a marginally different task and training strategy, which resulted in the animal producing very few (<1.5%) responses toward the cue-orthogonal locations. A different training strategy was used before data for the subsequent sessions were acquired, which encouraged the animal to make 3× more responses toward the cue-orthogonal locations (>5%), permitting behavioral analysis with SDT models. For this study, data were analyzed from the last 12 behavioral sessions for monkey B.

Neural data acquisition

Recordings in V4 were performed with 16-channel U-Probes (Plexon Inc., Dallas, TX). Data were filtered from 0.5 Hz to 8 kHz in hardware and were stored at a sampling rate of 40 kHz for offline analysis. The electrode array was left in place throughout the duration of each behavioral session, and post hoc analyses of the waveforms were used to isolate single and multiunits. Further details regarding the recordings, spike detection, and sorting procedures are provided in Steinmetz and Moore (*31*).

Eye position data acquisition and analysis

For monkey G, eye position was monitored with a scleral search coil in some sessions and an Eyelink 1000 infrared–based video eye tracking system in other sessions (*31*). For monkey B, eye position was monitored with the Eyelink 1000 in all sessions. Saccade data were stored for offline analysis. Saccade onset times and saccade target fixations were determined with the following procedure: Saccade onset times were recorded when gaze deviated beyond a small square box (~1.5° width) around the fixation dot and the speed of eye movement exceeded 250 degrees of visual angle per s. The eye position of the monkey 100 ms after the saccade onset was used to identify the saccade target (end point) fixation. For no-change responses, only trials in which the gaze did not deviate beyond the fixation box for a period of 800 ms after the stimuli reappeared were considered. Furthermore, we computed the average displacement of the eye position from fixation during the last 100 ms of the response window across no-change response trials, and rejected trials where this displacement was greater than the mean displacement by more than 3 SDs across trials. We used visual inspection to remove trials with irregular responses, such as double step saccades, in which the first fixation occurred in a visual quadrant different from the ultimate saccade target or averaging saccades that landed at intermediate locations between two visual targets.

Microsaccade detection algorithm

We detected microsaccades following the same approach as a recent study (*44*). After applying a bandstop filter to remove line noise at 60 Hz (second-order Butterworth IIR bandstop filter; lower and higher half power frequencies at 59 and 61 Hz), we smoothed the horizontal and vertical eye signals using rectangular windows of 10 ms width. Then, we calculated velocity from the eye positions using a finite difference approximation to the first derivative as: $vx(n) = Fs \times [x(n+2) + x(n+1) - x(n-1) - x(n-2)]/6$, where vx denotes the x component of the velocity vector, n denotes the sample number, Fs denotes the sampling rate, and $x(k)$ denotes the azimuthal position of the eye at sample k. The y component of the velocity vector was similarly computed based on the elevational position of the eye. Following this, we again smoothed the velocity signals using rectangular windows of 10 ms width. Microsaccades were detected using the algorithm described in Engbert and Kliegl (*43*). The algorithm computes velocity thresholds for each trial, as a multiple of the SD of the velocity distribution. The SD was calculated using a median estimator and multiplied by a constant C (for all results reported, $C = 4$). Furthermore, we considered only microsaccades with a minimum duration of 8 ms and an amplitude between 0.12 and 1.0 dva.

For each animal, we constructed average saccade vectors using the end points of the population of saccades to each target stimulus. We then projected each microsaccade vector on to these average saccade vectors and summed the projections across trials for each session; negative magnitudes of these projections, representing putative return or corrective microsaccades, were excluded from the sum.

Behavioral data analysis

Contingency tables

Animals' behavioral responses were organized into 5 × 5 stimulus-response contingency tables, with stimulus events—grating orientation change in one of four quadrants, or no change—along the rows and responses—saccade to one of the four stimulus locations, no saccade—along the columns. This contingency table was then reorganized so that all stimulus and response locations were sorted according to their position relative to the cue on each trial, as cued, cue-opposite, cue-ipsilateral, and cue-contralateral (fig. S1A). Given the antisaccade nature of the task, note that a saccade toward a grating stimulus location would indicate a report of change at the diametrically opposite grating stimulus. Each trial was classified into one of five types: as a hit, mislocalization, false alarm, miss, or correct rejection (fig. S1A).

m-ADC model fitting

The 5 × 5 stimulus response contingency table was fit with the m-ADC model (*6*, *10*) to estimate psychophysical parameters: sensitivity and criterion at each of the four locations. The m-ADC model extends conventional one-dimensional SDT into multiple dimensions (*41*, *73*) with the goal of distinguishing sensitivity and bias effects in attention tasks. The model is described in extensive detail and compared with alternative models in many previous studies (*6*, *8*–*10*, *58*, *74*).

Briefly, the multialternative decision is modeled in a multidimensional decision space, with four orthogonal decision variable axes representing sensory evidence for change at each of the four locations. Signal and noise distributions are modeled as multivariate Gaussians with an identity covariance matrix, and decisions are based on 10 planar decision surfaces (hyperplanes), which partition the four-dimensional decision space into five decision zones, each corresponding to a decision to report a change at one of the four locations, or no change. The noise (no-change) distribution is specified to have zero mean. The mean of the signal distribution along each decision axis is parameterized by the perceptual sensitivity (d') for detecting a change at the corresponding location. The distance from the origin of the four decision surfaces parallel to each coordinate hyperplane is parameterized by four criteria (c) for reporting a change at the corresponding location. Model parameters (d' and c) were estimated with maximum likelihood estimation; the fitting procedure has been described in detail previously (*8*, *10*). Here, we used a 4-ADC model as there were four potential locations of change.

Because of the challenging nature of the antisaccade task, both monkeys developed a strong oculomotor response bias. This bias overwhelmingly favored saccades toward the cue-opposite location (the most likely saccade location) on trials in which the orientation change occurred at one of the cue-orthogonal locations. This produced a large excess of mislocalization responses toward the cue-opposite location when changes occurred at the cue-orthogonal locations, as compared to false alarms (mislocalizations: monkey G: 0.44 ± 0.08, monkey B: 0.33 ± 0.05; false alarms: monkey G = 0.27 ± 0.01, monkey B = 0.18 ± 0.02; mean ± SD, across sessions). To accurately estimate psychophysical parameters while taking this response bias into account, we fit a modified version of the m-ADC model, incorporating a motor bias matrix (*6*). This fitting

was accomplished by multiplying the m-ADC estimated response proportions with a 4 × 4 motor bias matrix (fig. S1B), as follows

$$p(r|s) = \sum_{r'} p(r'|s) \times p(r|r')$$

where $p(r|s)$ represents the actual response proportions (actual proportion of responses to location r when the change occurred at location s), $p(r'|s)$ represents the response proportions in the m-ADC fit (estimated probability of response to location r' when the change occurred at location s), and $p(r|r')$ represents the motor bias (probability) for reporting location r when the m-ADC model indicated location r' for response. During fitting, each row in the motor bias matrix was constrained to sum to 1 (the law of probabilities). Thus, the motor bias matrix added 12 additional parameters to the m-ADC model fitting.

Psychophysical parameter estimation

For monkey G, orientation change magnitudes ranged across angles ranging from 2° to 90°. We binned these orientations into four bins: <45°, 45°, 67°, and 90°. For monkey B, orientation change magnitudes were always 45°, at both cued and uncued locations. Distinct d' parameters were estimated, one for each orientation change angle bin. A single criterion (c) was estimated for each location. All sensitivities reported correspond to 45° orientation changes for both monkeys. The number of parameters estimated for each monkey included 4 criterion parameters, $n_c + 3n_{uc}$ sensitivity parameters, and 12 parameters for the motor bias matrix, where n_c and n_{uc} denote the number of orientation change angle bins for the validly and invalidly cued locations, respectively (monkey G: $n_c = 4$, $n_{uc} = 2$; monkey B: $n_c = 1$, $n_{uc} = 1$). Maximum Likelihood (ML) estimation was performed to concurrently estimate both m-ADC parameters (sensitivity and criterion) and motor bias matrix parameters with data pooled across sessions and separately for each animal. In all cases, to ensure that ML estimation did not converge to a local minimum, we repeated the estimation with $n = 10$ random initializations of the parameters and chose the parameter configuration with best goodness-of-fit value; typically, this corresponded to the mode of the parameter configurations across the 10 runs. Zeros in the contingency table were replaced with a small value $[1/(2 \times N_{angles})]$ to ensure that the ML estimation did not diverge.

Following psychophysical parameter estimation, we computed the choice bias using the likelihood ratio measure (β) using an analytical relationship between β, d', and c for the m-ADC model derived previously [Banerjee *et al.* (*8*); their appendix]. Figure 1 (E and F) shows parameters obtained across individual sessions. Jackknife estimates of variance of sensitivity and bias parameters were obtained by leaving one session out at a time; motor bias parameters were kept constant based on the pooled session analysis. All sensitivity (d') and sensitivity modulation (MI-d') values reported in Fig. 1 (F and H) correspond to a change angle of 45°. The motor bias toward each location (r) was quantified as the sum of each column of the motor bias matrix [$\sum_{r'} p(r|r')$; fig. S1B]. Jackknife parameter estimates of motor bias parameters' variance (fig. S1C) were obtained by leaving one session out a time and estimating both m-ADC and motor bias parameters with the remaining $(n - 1)$ sessions.

Recording sites and sessions were chosen so that RFs of V4 units occurred in the lower-left visual quadrant (*31*). All analyses reported for V4 units included only units exhibiting visual responses or saccadic responses to the lower-left quadrant. To ensure correspondence between the behavioral and neural analyses, sensitivity and bias estimates were based on a contingency table with behavioral responses only on trials in which change events occurred in the lower-left quadrant (3101 of 12,597 change trials for monkey G; 2482 of 9782 change trials for monkey B); all no-change trials were included in these analyses (12,966 trials for monkey G; 10,293 trials for monkey B). Estimating sensitivity and bias with data from all trials (change and no change) revealed trends closely similar to those reported in Results.

To compare sensitivity and bias across cued and cue-opposite locations, we also computed an MI defined as the ratio of the difference of the value of the respective parameter between the cued (or cue-opposite) and cue-orthogonal locations to their sum. For example, $p\text{-MI}_{cued} = (p_{cued} - p_{ortho})/(p_{cued} + p_{ortho})$, where p_{cued} is either the sensitivity (d') or the bias (β) parameter at the cued location and p_{ortho} represents the average value of the respective parameter across the orthogonal (ipsilateral and contralateral) locations.

Median split of sessions based on psychophysical parameter values

To explore the correspondence between psychophysical parameters and neural activity, we divided the behavioral sessions into "high" and "low" sensitivity or high and low bias at the cued location (fig. S2, D and E), where a substantial proportion of changes occurred (~45% of all trials) in each session. Trials where change occurred at the RF were very rare at the cue-opposite location (0 to 15 trials per session, <2% overall), rendering it challenging to reliably estimate d' and bias at this location separately for each session. We performed a median split across sessions of the jackknife estimates of sensitivity (d', for 45° orientation changes) or the jackknife estimates of the likelihood-ratio bias (β), respectively. For these jackknife estimates, as before, the motor bias matrix was fixed to its value estimated from the pooled across sessions data. This median split into high and low d' (or bias) sessions was performed separately for each animal, and unit activity was pooled across each session type for analysis (see the "Analysis of V4 neural recordings" section).

Goodness-of-fit and statistical tests

We assessed goodness of fit of the 4-ADC model with the motor bias matrix to the measured behavioral responses, organized into a 5 × 5 contingency table, with a randomization test based on the chi-square statistic [see (*8*); their methods]. The test was performed by fitting the model to the data pooled across sessions, separately, for each monkey. The goodness-of-fit P value based on the randomization test was $P > 0.99$ for both monkeys. In addition, we also fit the contingency tables for individual sessions for each animal. In this case, we also observed good fits of the model to the data [monkey G: $P = 1.0$ (0.99 to 1.0), median (range), across $n = 18$ sessions; monkey B: $P = 1.0$ (0.98 to 1.0) across $n = 12$ sessions] (fig. S2C), indicating that the model fit did not deviate significantly from the observed response proportions in the contingency tables. In other words, the 4-ADC model, with the motor bias matrix, successfully accounted for the animals' behavior in this multialternative attention task.

Tests for significant differences between the psychometric parameters (hit rates and false-alarm rates) at the four different locations were performed with an ANOVA, with locations and sessions as factors, followed by a post hoc Tukey-Kramer correction for multiple comparisons. For the psychophysical parameters (sensitivity and bias) estimated on the pooled data, as opposed to the individual sessions, we established significance by performing a permutation test. To test for significant differences in sensitivity across locations, we adopted the following procedure: After estimating sensitivities

and criteria with the session-pooled contingency tables, we first set the sensitivity at each location to its average value across locations. We then estimated "null" conditional probabilities $p(r|s)$ with the m-ADC model using the criteria at the four locations and identical (average) sensitivity at each location. Following this, we performed multinomial sampling from the estimated null conditional probabilities and fit the m-ADC to each simulated contingency table, except that we permitted the model to only fit d' values, whereas the criteria remained fixed (to their original values). This procedure was repeated 1000 times to generate a null distribution of d' differences (or their modulation indices) across locations. Differences in the true d' estimates across locations were considered significant if they exceeded the 95th percentile of this null distribution of d' differences. To test for significant differences in choice bias across locations an identical procedure was followed, except that the null conditional probabilities $p(r|s)$ were estimated by setting the β (likelihood ratio bias) to its average value across locations, and fitting only the criteria when generating the null distribution.

Relevance of the motor bias matrix for fitting behavior

The goodness-of-fit testing results with the extended m-ADC model with the motor bias matrix showed that this model is sufficient to fit behavior in this cued, multialternative detection task. We tested whether incorporating the motor bias matrix was also necessary to model the animals' responses accurately, by performing four analyses: (i) a goodness-of-fit test for an m-ADC model without the motor bias matrix, (ii) a behavioral prediction analysis, (iii) an analysis that explored a more parsimonious version of the motor bias matrix, and (iv) an analysis that explored a more detailed version of the motor bias matrix.

The first analysis tested whether the motor bias matrix was necessary to model the animals' responses in this task. For this, we fit the standard 4-ADC model without incorporating the motor bias matrix. This model failed to accurately fit behavior ($P < 0.01$), indicating that the motor bias matrix was necessary for fitting the animals' responses. The goals of the second analysis were twofold: (i) to test whether the motor bias matrix was consistent across sessions and (ii) to test whether incorporating the motor bias matrix would improve the model's ability to predict the animals' behavior in held-out contingencies. For this, we fit the model based only on a subset of responses (9 of 25) in the contingency table, using either (i) hit (four contingencies), false-alarm (four contingencies), and correct rejection (one contingency) rates, or (ii) miss (four contingencies), false-alarm (four contingencies), and correct rejection (one contingency) rates. In each case, we split the trials into two folds by pooling the data across odd- and even-numbered trials, respectively. To ensure that each fold had appreciable number of trials at each location and change angle, for this analysis we included all trials, irrespective of whether the change occurred in the V4 units' RF. The motor bias matrix estimated from the full contingency table of the first fold was used for estimating parameters with the partial contingency table in the other fold. After fitting the model with a subset (9) of contingencies, we predicted the response proportions for the remaining 16 contingencies. Model parameter estimates across the two folds were correlated with robust (bend) correlations (*75*). The prediction analysis was repeated after excluding the motor bias matrix in the fitting. The results from this analysis are shown in fig. S2A. The third analysis tested whether more parsimonious solutions for the motor bias could fit the data equally well. For this, we estimated the parameters with maximum likelihood estimation as before, but including an additive penalty on the Frobenius norm ($||M||_2$) of the motor bias matrix weighted by a factor λ. Thus, the objective function was to maximize [−log (likelihood) + $\lambda||M||_2$)]. Note that because each row of the motor bias matrix is constrained to sum to 1 [$\Sigma_{r'} p(r|r') = 1$], the minimum penalty solution corresponds to an equal value (0.25) for all entries, indicating uniform motor bias toward all locations. The results of this analysis are shown in fig. S2B. Note that, in our model, multiplying the m-ADC contingency table with the motor bias matrix only affects the Go (saccade) response proportions corresponding to hits, false alarms, and mislocalizations. Setting the last row and last column of the motor bias matrix to zero (except for the corner element, which is set to 1) (fig. S1B) ensures that NoGo (no saccade) response proportions, corresponding to misses and correct rejections, are unaffected by multiplication with the motor bias matrix. The fourth analysis tested whether by not imposing this form on the motor bias matrix, parameter estimates were rendered degenerate (nonidentifiable model) (*10*). To illustrate this empirically, we fit the contingency table for each monkey (pooled across sessions) with a 5 × 5 motor-bias matrix, where the last row and column of the motor bias matrix were not fixed to zeros (again, we ensured that each row summed to 1 based on the law of probabilities). We ran 10 iterations of this model, as well as the default model, with different initial conditions and compared the consistency of the parameter estimates across the two models. Across 10 iterations of fitting the 5 × 5 motor bias matrix model, the model converged to widely different parameter estimates on each iteration, with >6 orders of magnitude higher SD as compared to the default model. In other words, the extended m-ADC model, with the motor bias matrix, was necessary and sufficient to accurately model animals' behavior in this attention task.

Comparing parameter estimates with a similarity choice model

To test whether the specific sensitivity and bias parameter estimates reported in this study were predicated on underlying assumptions in the m-ADC model, we also estimated these same parameters with a similarity choice model (*76*). Briefly, the similarity choice model fits multialternative behavioral data by factoring the underlying response proportions into sensitivity and bias parameters (Materials and Methods); in this sense, it is unlike the m-ADC model, which is a latent variable model within the framework of SDT.

Whereas the extended m-ADC model fit the 5 × 5 contingency table with 4 sensitivity parameters per change angle, 4 choice bias, and 12 motor bias parameters, the choice theory model fit the contingency table with 10 sensitivity parameters per change angle and 4 bias parameters. In addition, the similarity choice model does not distinguish between choice bias and motor bias parameters. Model fitting and evaluation have been described previously (*8*). We compared parameter estimates from the similarity choice model with those from the m-ADC model at the different locations. Both the similarity choice model estimates and the m-ADC model estimates were obtained by fitting trials pooled across angles and sessions. The results from this analysis are shown in fig. S3.

Effect of criterion changes on overall accuracy in multialternative detection tasks

For simplicity of illustration, we simulated a 2-ADC task, with two potential change locations, with decision variable distributions generated with a 2-ADC model. This model incorporates three responses—change at the cued location, change at the uncued location, or no change. Fifty percent of all trials were simulated as change

trials, and the remaining 50% were no-change trials. The prior probability of change at the cued and uncued locations was fixed to 90 and 10%, respectively. These values correspond to cue validities and trial proportions in the actual behavioral task on which the monkeys were trained (see the "Behavioral task and data acquisition" section). Choice criteria at the uncued locations were fixed to one of three values ($cc_{uncued} = -1.0$, 0.0, or 1.0), and for each of these parameter combinations, choice criteria at the cued location were varied between −3.0 and 3.0 in steps of 0.1. Sensitivities were fixed at both cued and uncued locations to a value of 1.0 ($d'_{cued} = d'_{uncued} = 1.0$).

Simulated response proportions in a 3 × 3 contingency table were generated with 2-ADC model equations [see (*6*); their eqs. 2 and 19 to 24), based on these values of the sensitivity and criteria at the cued and uncued locations. Overall percent correct was computed from these simulated responses as the average of the proportion of hits on change trials at the cued, at the uncued location, and the proportion of correct rejection responses on no-change trials. The results of the simulations are shown in fig. S4.

Analysis of V4 neural recordings

Characterization of units

Single-unit and multiunit recordings were combined for analyses. V4 units with an average FR of less than 0.1 Hz were excluded from all analyses. V4 units across all cortical layers were analyzed regardless of depth of recording on the U-Probe (total of $n = 297$ V4 units in monkey G and 167 units in monkey B). V4 recordings were performed for all behavioral sessions analyzed in this study (18 sessions for monkey G and 12 sessions for monkey B).

Analysis of FRs

As with the psychophysical parameters, we defined modulation indices of FRs for the cued and cue-opposite conditions. For example, the FR MI for the cued condition was defined as $MI_{FRcued} = (f_{cued} - f_{ortho})/(f_{cued} + f_{ortho})$, where f_{cued} and f_{ortho} represent the FR for the cued condition and for the cued-orthogonal conditions (average of ipsilateral and contralateral locations), respectively. To examine the dynamics of firing relative to cue onset, the MI was computed in 500-ms moving windows locked to cue onset with a 50-ms shift (e.g., Fig. 2, A and C). Statistical analyses during the cue epoch were performed in two windows. The MI was computed in two windows: (i) from 500 ms after cue onset until the end of the cue epoch (e.g., Fig. 2, B and D) and (ii) from 400 ms before blank onset until blank onset; the latter window is more relevant for capturing changes in neural activity linked to psychophysical parameter (sensitivity and bias) modulations because it is closer to the change event and also avoids large transients associated with the blank onset itself. We tested for significant difference of the FR MI (MI_{FR}) from zero at each location and also for the difference of MI_{FR} across cued and cue-opposite conditions with a nonparametric Wilcoxon signed rank test. MI_{FR} differences between the high and low d' (or high and low bias) sessions were tested with the Mann-Whitney *U* test. We also quantified the effect size of the differences between MI_{FR} values across high and low d' sessions (or high- and low-bias sessions) with a Cohen's *d* metric defined as the difference between the mean MI_{FR} for units in the high and low conditions divided by their common SD (*77*).

Analysis of Fano factor

The trial-to-trial variability in FR for each unit was quantified using the Fano factor, calculated as the variance divided by the mean of the spike count across trials during the cue epoch (500 ms after cue onset until end of cue epoch). As in Steinmetz and Moore (*31*), the Fano factor was computed separately for each RF stimulus orientation and averaged across these orientations for each stimulus location (relative to the cue).

We computed the Fano factor MI (MI_{FF}) for the cued (or cue-opposite) conditions, as before, as the ratio of the difference in the value of the parameter between the cued (or cue-opposite) and cue-orthogonal conditions to their sum. As with the FR analyses, MI_{FF} was compared for significant differences across the high and low *d*' (or high and low bias) sessions with a nonparametric Mann-Whitney *U* test.

Tuning curve analysis

For the tuning curve analysis, we followed a similar procedure to (*46*). We included units that were significantly modulated ($P < 0.0001$, Kruskal-Wallis test of FRs grouped by orientation of stimulus presented in the RF) 50 to 350 ms after stimulus onset. A Gaussian was fit to the average activity (normalized by the maximum activity across conditions) of each significantly tuned unit as described below

$$r(\theta) = A \times e^{-\left[\frac{(\theta-\mu)}{\sigma}\right]^2} + b$$

where the amplitude (A), mean (μ), width (σ), and baseline (b) are the parameters of the tuning curve. We used the MATLAB lsqcurvefit function to fit the function. The upper bound for the mean was set to π. We fit the Gaussian for 100 iterations, each with a random initial condition and computed the coefficient of determination (R^2). The fitting was terminated when R^2 crossed a value of 0.7. Only units with $R^2 > 0.7$ were considered for further analyses. The MI for the estimated parameters was computed after splitting the data into high and low sessions as described previously.

We also plotted the normalized FRs for the cued condition against the corresponding values for the cue-orthogonal condition for each of the eight stimulus orientations, and fit a linear model using the MATLAB robustfit function. We used this to obtain the slope and intercept parameters after splitting the data into high and low sessions. An intercept significantly greater than zero implies an additive increase in baseline, and a slope significantly greater than 1 corresponds to a multiplicative gain in amplitude for the cued, relative to the cue-orthogonal, condition.

Noise correlation analysis

We tested whether noise correlations (r-sc) across trials between pairs of V4 units would show signatures of sensitivity or bias modulations. Noise correlation between each pair of simultaneously recorded units was computed as the Pearson correlation coefficient of their FRs estimated in the same set of two windows as with FRs: (i) from 500 ms after cue onset until the end of the cue epoch and (ii) from 400 ms before the blank onset until blank onset. These correlation coefficients were computed separately for each stimulus orientation and cue condition and then averaged across stimulus orientations. The MI of noise correlations was subsequently computed as

$$\mathrm{MI(cued)} = \frac{r_{sc}(\mathrm{cued}) - r_{sc}(\mathrm{ortho})}{\sqrt{r_{sc}(\mathrm{cued})^2 + r_{sc}(\mathrm{ortho})^2}}$$

The stimulus evoked response of each unit was computed as the difference in FRs during the stimulus presentation epoch (60 to 260 ms after stimulus onset) and the fixation epoch [FR(stimulus epoch)

− FR(fixation)]. Pairs were binned on the basis of the geometric mean of the evoked response of the two units in four bins: 5 to 10, 10 to 20, 20 to 30, and >30 spikes/s. For all comparisons across conditions, we only considered pairs with >5 spikes/s evoked response. To establish significance for comparisons of noise correlation across high and low sensitivity (or choice bias) sessions, the high and low labels were randomly shuffled 10,000 times to generate a null distribution of the difference between the means, against which the observed difference in means was compared to obtain a *P* value.

Layer-wise analysis

We performed layer assignments following the same methods as in previously published work (*46*, *78*). Briefly, laminar depths were assigned to each recording from the 16 electrode channels relative to a common CSD marker in each recording session. The details can be found in Pettine *et al.* (*46*). For the analyses reported in the Results, we divided units as belonging to superficial (II to IV) and deep (V/VI) layers: the boundary between the two laminar compartments was taken as the depth below the first current sink that was followed by a reversal to the current source, typically within <100 ms of stimulus onset. Thus, the superficial compartment included what was likely input layer IV (*19*). For a small number of sessions (6 of 30), we observed multiple sink bands. For these sessions, we placed the boundary between the superficial and deep layers typically below the upper sink band; this resulted in superficial-deep boundary placements that lay within the normative range of the boundary depths observed in all other sessions. MI_{FR} and $MI_{r\text{-}sc}$ were subsequently computed for superficial- and deep-layer units separately. Potential challenges with distinguishing layer III from layer IV based on CSD profiles has been discussed in earlier work [Steinmetz (*79*), pp. 108–109, their figures 4 to 10]. Briefly, the reasons include challenges with uniquely mapping CSD profile thickness to cortical thickness, due to potential compression of cortical tissue around the electrode, as well as ambiguity with the timing of the earliest visual inputs reaching V4 (ventral stream regions versus pulvinar nucleus of the thalamus) (*80*–*82*). Nevertheless, we sought to identify the input layer based on CSD markers reported in literature (*19*); this was feasible in a subset of sessions (22 of 30) in which layer IV could be clearly demarcated from layers II and III (fig. S7A). MI_{FR} and $MI_{r\text{-}sc}$ were, thus, also computed for the input units, where possible. These rules for layer assignment were consistently applied throughout all recording sessions.

Statistical analysis

The details of all statistical tests performed are described in Materials and Methods sections above. The details regarding the error bars and shaded regions are described in the figure legends.

Supplementary Materials

This PDF file includes:

Figs. S1 to S8

REFERENCES AND NOTES

1. H. S. Bashinski, V. R. Bacharach, Enhancement of perceptual sensitivity as the result of selectively attending to spatial locations. *Percept. Psychophys.* **28**, 241–248 (1980).
2. M. I. Posner, Orienting of attention. *Q. J. Exp. Psychol.* **32**, 3–25 (1980).
3. J. Duncan, Selective attention and the organization of visual information. *J. Exp. Psychol. Gen.* **113**, 501–517 (1984).
4. S. J. Luck, S. A. Hillyard, M. Mouloua, H. L. Hawkins, Mechanisms of visual–spatial attention: Resource allocation or uncertainty reduction? *J. Exp. Psychol. Hum. Percept. Perform.* **22**, 725–737 (1996).
5. T. J. Buschman, S. Kastner, From behavior to neural dynamics: An integrated theory of attention. *Neuron* **88**, 127–144 (2015).
6. D. Sridharan, N. A. Steinmetz, T. Moore, E. I. Knudsen, Does the superior colliculus control perceptual sensitivity or choice bias during attention? Evidence from a multialternative decision framework. *J. Neurosci.* **37**, 480–511 (2017).
7. E. I. Knudsen, Neural circuits that mediate selective attention: A comparative perspective. *Trends Neurosci.* **41**, 789–805 (2018).
8. S. Banerjee, S. Grover, S. Ganesh, D. Sridharan, Sensory and decisional components of endogenous attention are dissociable. *J. Neurophysiol.* **122**, 1538–1554 (2019).
9. V. Sagar, R. Sengupta, D. Sridharan, Dissociable sensitivity and bias mechanisms mediate behavioral effects of exogenous attention. *Sci. Rep.* **9**, 12657 (2019).
10. D. Sridharan, N. A. Steinmetz, T. Moore, E. I. Knudsen, Distinguishing bias from sensitivity effects in multialternative detection tasks. *J. Vis.* **14**, 16–16 (2014).
11. T. B. Crapse, H. Lau, M. A. Basso, A role for the superior colliculus in decision criteria. *Neuron* **97**, 181–194.e6 (2018).
12. T. Z. Luo, J. H. R. Maunsell, Attentional changes in either criterion or sensitivity are associated with robust modulations in lateral prefrontal cortex. *Neuron* **97**, 1382–1393.e7 (2018).
13. T. Z. Luo, J. H. R. Maunsell, Neuronal modulations in visual cortex are associated with only one of multiple components of attention. *Neuron* **86**, 1182–1188 (2015).
14. C. J. McAdams, J. H. R. Maunsell, Effects of attention on orientation-tuning functions of single neurons in macaque cortical area V4. *J. Neurosci.* **19**, 431–441 (1999).
15. J. H. Reynolds, T. Pasternak, R. Desimone, Attention increases sensitivity of V4 neurons. *Neuron* **26**, 703–714 (2000).
16. S. Treue, J. C. M. Trujillo, Feature-based attention influences motion processing gain in macaque visual cortex. *Nature* **399**, 575–579 (1999).
17. M. R. Cohen, J. H. R. Maunsell, Attention improves performance primarily by reducing interneuronal correlations. *Nat. Neurosci.* **12**, 1594–1600 (2009).
18. J. F. Mitchell, K. A. Sundberg, J. H. Reynolds, Spatial attention decorrelates intrinsic activity fluctuations in macaque area V4. *Neuron* **63**, 879–888 (2009).
19. A. S. Nandy, J. J. Nassi, J. H. Reynolds, Laminar organization of attentional modulation in macaque visual area V4. *Neuron* **93**, 235–246 (2017).
20. A. M. Ni, D. A. Ruff, J. J. Alberts, J. Symmonds, M. R. Cohen, Learning and attention reveal a general relationship between population activity and behavior. *Science* **359**, 463–465 (2018).
21. J. H. R. Maunsell, Neuronal mechanisms of visual attention. *Annu. Rev. Vis. Sci.* **1**, 373–391 (2015).
22. M. Carrasco, Visual attention: The past 25 years. *Vision Res.* **51**, 1484–1525 (2011).
23. T. Moore, M. Zirnsak, Neural mechanisms of selective visual attention. *Annu. Rev. Psychol.* **68**, 47–72 (2017).
24. H. Deubel, W. X. Schneider, Saccade target selection and object recognition: Evidence for a common attentional mechanism. *Vision Res.* **36**, 1827–1837 (1996).
25. J. E. Hoffman, B. Subramaniam, The role of visual attention in saccadic eye movements. *Percept. Psychophys.* **57**, 787–795 (1995).
26. T. Moore, K. M. Armstrong, Selective gating of visual signals by microstimulation of frontal cortex. *Nature* **421**, 370–373 (2003).
27. T. Moore, M. Fallah, Control of eye movements and spatial attention. *Proc. Natl. Acad. Sci. U.S.A.* **98**, 1273–1276 (2001).
28. C. C. Ruff, S. Bestmann, F. Blankenburg, O. Bjoertomt, O. Josephs, N. Weiskopf, R. Deichmann, J. Driver, Distinct causal influences of parietal versus frontal areas on human visual cortex: Evidence from concurrent TMS–fMRI. *Cereb. Cortex* **18**, 817–827 (2008).
29. D. E. Winkowski, E. I. Knudsen, Top-down gain control of the auditory space map by gaze control circuitry in the barn owl. *Nature* **439**, 336–339 (2006).
30. H.-H. Li, J. Pan, M. Carrasco, Different computations underlie overt presaccadic and covert spatial attention. *Nat. Hum. Behav.* **5**, 1418–1431 (2021).
31. N. A. Steinmetz, T. Moore, Eye movement preparation modulates neuronal responses in area V4 when dissociated from attentional demands. *Neuron* **83**, 496–506 (2014).
32. J. W. Bisley, M. E. Goldberg, Attention, intention, and priority in the parietal lobe. *Annu. Rev. Neurosci.* **33**, 1–21 (2010).
33. L. H. Snyder, A. P. Batista, R. A. Andersen, Coding of intention in the posterior parietal cortex. *Nature* **386**, 167–170 (1997).
34. J. Cavanaugh, R. H. Wurtz, Subcortical modulation of attention counters change blindness. *J. Neurosci.* **24**, 11236–11243 (2004).
35. S. J. Luck, L. Chelazzi, S. A. Hillyard, R. Desimone, Neural mechanisms of spatial selective attention in areas V1, V2, and V4 of macaque visual cortex. *J. Neurophysiol.* **77**, 24–42 (1997).
36. C. J. McAdams, J. H. R. Maunsell, Attention to both space and feature modulates neuronal responses in macaque area V4. *J. Neurophysiol.* **83**, 1751–1755 (2000).
37. H. Spitzer, R. Desimone, J. Moran, Increased attention enhances both behavioral and neuronal performance. *Science* **240**, 338–340 (1988).
38. T. Williford, J. H. R. Maunsell, Effects of spatial attention on contrast response functions in macaque area V4. *J. Neurophysiol.* **96**, 40–54 (2006).

39. K. M. Armstrong, M. H. Chang, T. Moore, Selection and maintenance of spatial information by frontal eye field neurons. *J. Neurosci.* **29**, 15621–15629 (2009).
40. J. L. Herrero, M. A. Gieselmann, M. Sanayei, A. Thiele, Attention-induced variance and noise correlation reduction in macaque V1 Is mediated by NMDA receptors. *Neuron* **78**, 729–739 (2013).
41. D. M. Green, J. A. Swets, *Signal Detection Theory and Psychophysics* (Wiley, 1966).
42. R. D. Luce, A choice theory analysis of similarity judgments. *Psychometrika* **26**, 151–163 (1961).
43. R. Engbert, R. Kliegl, Microsaccades uncover the orientation of covert attention. *Vision Res.* **43**, 1035–1045 (2003).
44. E. Lowet, B. Gomes, K. Srinivasan, H. Zhou, R. J. Schafer, R. Desimone, Enhanced neural processing by covert attention only during microsaccades directed toward the attended stimulus. *Neuron* **99**, 207–214.e3 (2018).
45. X. Li, Z.-L. Lu, B. S. Tjan, B. A. Dosher, W. Chu, Blood oxygenation level-dependent contrast response functions identify mechanisms of covert attention in early visual areas. *Proc. Natl. Acad. Sci. U.S.A.* **105**, 6202–6207 (2008).
46. W. W. Pettine, N. A. Steinmetz, T. Moore, Laminar segregation of sensory coding and behavioral readout in macaque V4. *Proc. Natl. Acad. Sci. U.S.A.* **116**, 14749–14754 (2019).
47. B. B. Averbeck, P. E. Latham, A. Pouget, Neural correlations, population coding and computation. *Nat. Rev. Neurosci.* **7**, 358–366 (2006).
48. G. Rizzolatti, L. Riggio, I. Dascola, C. Umiltá, Reorienting attention across the horizontal and vertical meridians: Evidence in favor of a premotor theory of attention. *Neuropsychologia* **25**, 31–40 (1987).
49. B. Fischer, R. Boch, Enhanced activation of neurons in prelunate cortex before visually guided saccades of trained rhesus monkeys. *Exp. Brain Res.* **44**, 129–137 (1981).
50. T. Moore, A. S. Tolias, P. H. Schiller, Visual representations during saccadic eye movements. *Proc. Natl. Acad. Sci. U.S.A.* **95**, 8981–8984 (1998).
51. M. Rolfs, M. Carrasco, Rapid simultaneous enhancement of visual sensitivity and perceived contrast during saccade preparation. *J. Neurosci.* **32**, 13744–13752a (2012).
52. Z. M. Hafed, J. J. Clark, Microsaccades as an overt measure of covert attention shifts. *Vision Res.* **42**, 2533–2545 (2002).
53. R. J. Krauzlis, A. Bollimunta, F. Arcizet, L. Wang, Attention as an effect not a cause. *Trends Cogn. Sci.* **18**, 457–464 (2014).
54. J. K. Baruni, B. Lau, C. D. Salzman, Reward expectation differentially modulates attentional behavior and activity in visual area V4. *Nat. Neurosci.* **18**, 1656–1663 (2015).
55. A. I. Jasper, S. Tanabe, A. Kohn, Predicting perceptual decisions using visual cortical population responses and choice history. *J. Neurosci.* **39**, 6714–6727 (2019).
56. V. Wyart, A. C. Nobre, C. Summerfield, Dissociable prior influences of signal probability and relevance on visual contrast sensitivity. *Proc. Natl. Acad. Sci. U.S.A.* **109**, 3593–3598 (2012).
57. E. I. Knudsen, J. S. Schwarz, P. F. Knudsen, D. Sridharan, Space-specific deficits in visual orientation discrimination caused by lesions in the midbrain stimulus selection network. *Curr. Biol.* **27**, 2053–2064.e5 (2017).
58. V. Sreenivasan, D. Sridharan, Subcortical connectivity correlates selectively with attention's effects on spatial choice bias. *Proc. Natl. Acad. Sci. U.S.A.* **116**, 19711–19716 (2019).
59. J. Martinez-Trujillo, R. A. Gulli, Dissecting modulatory effects of visual attention in primate lateral prefrontal cortex using signal detection theory. *Neuron* **97**, 1208–1210 (2018).
60. S. Zhang, M. Xu, T. Kamigaki, J. P. Hoang Do, W.-C. Chang, S. Jenvay, K. Miyamichi, L. Luo, Y. Dan, Long-range and local circuits for top-down modulation of visual cortex processing. *Science* **345**, 660–665 (2014).
61. G. H. Denfield, A. S. Ecker, T. J. Shinn, M. Bethge, A. S. Tolias, Attentional fluctuations induce shared variability in macaque primary visual cortex. *Nat. Commun.* **9**, 2654 (2018).
62. T. A. Engel, N. A. Steinmetz, M. A. Gieselmann, A. Thiele, T. Moore, K. Boahen, Selective modulation of cortical state during spatial attention. *Science* **354**, 1140–1144 (2016).
63. E. A. Buffalo, P. Fries, R. Landman, T. J. Buschman, R. Desimone, Laminar differences in gamma and alpha coherence in the ventral stream. *Proc. Natl. Acad. Sci.* **108**, 11262–11267 (2011).
64. C. D. Gilbert, T. N. Wiesel, Functional organization of the visual cortex. *Prog. Brain Res.* **58**, 209–218 (1983).
65. N. T. Markov, J. Vezoli, P. Chameau, A. Falchier, R. Quilodran, C. Huissoud, C. Lamy, P. Misery, P. Giroud, S. Ullman, P. Barone, C. Dehay, K. Knoblauch, H. Kennedy, Anatomy of hierarchy: Feedforward and feedback pathways in macaque visual cortex. *J. Comp. Neurol.* **522**, 225–259 (2014).
66. G. R. Leichnetz, R. F. Spencer, S. G. P. Hardy, J. Astruc, The prefrontal corticotectal projection in the monkey; an anterograde and retrograde horseradish peroxidase study. *Neuroscience* **6**, 1023–1041 (1981).
67. J. C. Anderson, H. Kennedy, K. A. C. Martin, Pathways of attention: Synaptic relationships of frontal eye field to V4, lateral intraparietal cortex, and area 46 in macaque monkey. *J. Neurosci.* **31**, 10872–10881 (2011).
68. L. Chelazzi, E. K. Miller, J. Duncan, R. Desimone, A neural basis for visual search in inferior temporal cortex. *Nature* **363**, 345–347 (1993).
69. S. Treue, J. H. R. Maunsell, Effects of attention on the processing of motion in macaque middle temporal and medial superior temporal visual cortical areas. *J. Neurosci.* **19**, 7591–7602 (1999).
70. A. Zénon, R. J. Krauzlis, Attention deficits without cortical neuronal deficits. *Nature* **489**, 434–437 (2012).
71. L. Wollenberg, H. Deubel, M. Szinte, Visual attention is not deployed at the endpoint of averaging saccades. *PLoS Biol.* **16**, e2006548 (2018).
72. T. Moore, M. H. Chang, Presaccadic discrimination of receptive field stimuli by area V4 neurons. *Vision Res.* **49**, 1227–1232 (2009).
73. F. G. Ashby, F. A. Soto, Multidimensional signal detection theory, in *Oxford Handbook of Computational and Mathematical Psychology* (2015), pp. 13–34.
74. L. P. Lovejoy, R. J. Krauzlis, Changes in perceptual sensitivity related to spatial cues depends on subcortical activity. *Proc. Natl. Acad. Sci. U.S.A.* **114**, 6122–6126 (2017).
75. R. R. Wilcox, The percentage bend correlation coefficient. *Psychometrika* **59**, 601–616 (1994).
76. R. D. Luce, *Individual Choice Behavior: A Theoretical Analysis* (Courier Corporation, 2012).
77. J. Cohen, *Statistical Power Analysis for the Behavioral Sciences* (Academic Press, 2013).
78. Y.-L. Shi, N. A. Steinmetz, T. Moore, K. Boahen, T. A. Engel, Cortical state dynamics and selective attention define the spatial pattern of correlated variability in neocortex. *Nat. Commun.* **13**, 44 (2022).
79. N. A. Steinmetz, "Circuits Underlying Visual Attention in Primate Neocortex," thesis, Stanford University, Stanford, CA (2014).
80. S. M. Sherman, R. W. Guillery, The role of the thalamus in the flow of information to the cortex. *Philos. Trans. R. Soc. Lond. B Biol. Sci.* **357**, 1695–1708 (2002).
81. C.-M. Chen, P. Lakatos, A. S. Shah, A. D. Mehta, S. J. Givre, D. C. Javitt, C. E. Schroeder, Functional anatomy and Interaction of fast and slow visual pathways in macaque monkeys. *Cereb. Cortex* **17**, 1561–1569 (2007).
82. B. J. Hansen, V. Dragoi, Adaptation-induced synchronization in laminar cortical circuits. *Proc. Natl. Acad. Sci. U.S.A.* **108**, 10720–10725 (2011).

Acknowledgments

Funding: This research was supported by a Department of Biotechnology/Welcome Trust India Alliance Intermediate fellowship (IA/I/15/2/502089); a DST Swarna Jayanti Fellowship, a Science and Engineering Research Board Early Career award (ECR/2016/000403); a Pratiksha Trust intramural grant, a Department of Biotechnology–Indian Institute of Science Partnership Program grant; an India Trento Partnership Program grant (all to D.S.), an NSF graduate research fellowship (to N.S.), and an NIH EY014924 grant (to T.M.). **Author contributions:** D.S. conceived the study. T.M. and N.S. designed the experiments. N.S. performed the experiments. A.N.C., A.V., and P.G. developed analysis tools and analyzed the data. D.S. wrote the manuscript with inputs from all authors. **Competing interests:** D.S. is a research consultant at Google. All other authors declare that they have no competing interests. **Data and materials availability:** All data needed to evaluate the conclusions in the paper are present in the paper and/or the Supplementary Materials. The data and custom MATLAB code for reproducing all figures and tables in the paper is available at the following URL: https://doi.org/10.6084/m9.figshare.23897040.v3.

Submitted 8 April 2023
Accepted 4 January 2024
Published 2 February 2024
10.1126/sciadv.adi0645